

The formation of lithium-rich pegmatites through multi-stage melting

Tracking no: G51633R

Authors:

Lot Koopmans (University of Oxford), Tania Martins (Manitoba Geological Survey), Robert Linnen (Western University), Nicholas Gardiner (University of St Andrews), Catriona Breasley (University of British Columbia), Richard Palin (University of Oxford), Lee Groat (University of British Columbia), David Silva (University of British Columbia), and Laurence Robb (University of Oxford)

Abstract:

Lithium-cesium-tantalum type pegmatites - the primary source of lithium - crystallize from highly evolved, volatile- felsic melts that incorporated crustal material in their source. Pegmatites are classically thought to form either from extreme fractionation of a parental granite body or via low-degree partial melting of a metamorphic rock (anatectic-origin). However, the processes that lead to the formation of economic lithium pegmatite deposits remain enigmatic, since precipitation of lithium ore minerals requires melt lithium concentrations in excess of 5000 ppm - approximately 500 times upper crustal abundances. Here, we use petrological modeling to quantify lithium enrichment in an anatectic-origin scenario and show that it is primarily driven by the relative stability of residual biotite and muscovite at medium to high pressures (~8 kbar), and biotite and cordierite at low pressures (~3 kbar). We show anatexis of an average lithium-enriched metasedimentary source cannot sufficiently elevate the lithium content of the ensuing melt to form economic deposits; however, if this first-generation melt - now crystallized as granitic crust - is re-melted, the second-generation melt will be sufficiently concentrated in lithium to crystallize lithium ore minerals. We propose a petrogenetic model for anatectic-origin lithium pegmatites, in which a region experiences at least two stages of partial melting, ultimately generating lithium-rich melts without invoking extensive fractional crystallization. This mechanism can account for both the occurrence of unzoned lithium pegmatites and explains why economic pegmatites in many terranes are younger than their inferred source granites.

1 The formation of lithium-rich pegmatites through multi-stage
2 melting

3 **Lot Koopmans¹, Tania Martins², Robert Linnen³, Nicholas J. Gardiner⁴, Catriona M.
4 Breasley⁵, Richard M. Palin¹, Lee A. Groat⁵, David Silva⁵, and Laurence J. Robb¹**

5 *¹Department of Earth Sciences, University of Oxford, 3 South Parks Road, Oxford, OX1 3AN
6 United Kingdom*

7 *²Manitoba Geological Survey, 360-1395 Ellice Avenue, Winnipeg, Manitoba, Canada, R3G 3P2*

8 *³Department of Earth Sciences, Western University, 1151 Richmond Street N., London, Ontario,
9 Canada, N6A 5B7*

10 *⁴School of Earth & Environmental Sciences, University of St Andrews, Bute Building, Queen's
11 Terrace, St Andrews, KY16 9TS, United Kingdom*

12 *⁵Department of Earth, Ocean, & Atmospheric Sciences, University of British Columbia, 2207
13 Main Mall, Vancouver, British Columbia, Canada, V6T 1Z4*

14 **ABSTRACT**

15 Lithium-cesium-tantalum type pegmatites – the primary source of lithium – crystallize from
16 highly evolved, volatile- felsic melts that incorporated crustal material in their source. Pegmatites
17 are classically thought to form either from extreme fractionation of a parental granite body or via
18 low-degree partial melting of a metamorphic rock (anatectic-origin). However, the processes that
19 lead to the formation of economic lithium pegmatite deposits remain enigmatic, since
20 precipitation of lithium ore minerals requires melt lithium concentrations in excess of 5000 ppm
21 – approximately 500 times upper crustal abundances. Here, we use petrological modeling to
22 quantify lithium enrichment in an anatectic-origin scenario and show that it is primarily driven

23 by the relative stability of residual biotite and muscovite at medium to high pressures (~8 kbar),
24 and biotite and cordierite at low pressures (~3 kbar). We show anatexis of an average lithium-
25 enriched metasedimentary source cannot sufficiently elevate the lithium content of the ensuing
26 melt to form economic deposits; however, if this first-generation melt – now crystallized as
27 granitic crust – is re-melted, the second-generation melt will be sufficiently concentrated in
28 lithium to crystallize lithium ore minerals. We propose a petrogenetic model for anatectic-origin
29 lithium pegmatites, in which a region experiences at least two stages of partial melting,
30 ultimately generating lithium-rich melts without invoking extensive fractional crystallization.
31 This mechanism can account for both the occurrence of unzoned lithium pegmatites and explains
32 why economic pegmatites in many terranes are younger than their inferred source granites.

33

34 INTRODUCTION

35 Lithium–cesium–tantalum (LCT) pegmatites are formed from highly fractionated melts (Černý,
36 1991) and dominate global lithium (Li) production (U.S. Geological Survey, 2023). LCT
37 pegmatites first appeared in the Neoproterozoic (c. 2.8 Ga), are dominantly hosted in greenschist- to
38 amphibolite-grade supracrustal rocks (Dittrich et al., 2019), and retain geochemical signatures
39 which imply their genesis involved reworking of existing (typically metasedimentary) crust
40 (Černý, 1991). However, fundamental questions remain regarding how these evolved rocks
41 become highly concentrated in Li, since the primary extractable Li ore minerals – the Li-
42 aluminosilicates spodumene and petalite – only crystallize when melt Li contents exceed 5000
43 ppm (London, 1984; Maneta et al., 2015), representing an enrichment of ca. 500 times above
44 ordinary crustal abundances (Taylor and McLennan, 2003). Furthermore, to be economically
45 viable, an economic Li-pegmatite deposit must contain a sufficiently large mineralized zone

46 (Bradley and Mccauley, 2017), the extent of which is controlled by the initial Li concentration in
47 the emplaced pegmatitic melt (London, 2014).

48 In general, concentrating incompatible elements such as Li within a small-volume melt
49 fraction occurs through either (i) high-degree crystal fractionation of a larger body of magma, or
50 (ii) siphoning low-degree (e.g., 7–10%) partial melts away from a source rock undergoing
51 anatexis. These contrasting processes underpin two proposed LCT pegmatite petrogenetic
52 models: (1) extreme fractionation of a granitic magma that carries a typical (crustal) Li
53 concentration, generating a minor volatile- and metal-rich melt fraction which migrates from the
54 source region and ultimately crystallizes as a pegmatite (Cameron et al., 1949; Jahns, 1953;
55 Černý, 1991; Černý et al., 2005), or (2) low-degree partial melting of Li-rich host rocks during
56 prograde metamorphism (‘anatectic origin’), generating a volatile-rich melt that does not require
57 significant additional fractionation (Stewart, 1978; Simmons et al., 1995; Shaw et al., 2016;
58 Müller et al., 2017).

59 Recent research has focused on the anatectic model as a viable mechanism to form
60 economic pegmatite deposits (Müller et al., 2017; Kunz et al., 2022; Knoll et al., 2023). Here, we
61 use petrological modelling to quantify the extent of Li enrichment during crustal melting of
62 metasedimentary protoliths, and then assess how subsequent melting of their crystallized
63 magmatic products might serve to further concentrate Li in newly formed melt fractions. Our
64 results imply that multi-step anatexis in long-lived orogenic systems can act as a highly efficient
65 mechanism to produce economic grade LCT pegmatites.

66

67 **MODELING LI ENRICHMENT DURING CRUSTAL ANATEXIS**

68 Lithium in metasedimentary rocks is primarily hosted in biotite, muscovite, cordierite, and
69 staurolite (Simons et al., 2017; Kunz et al., 2022; Knoll et al., 2023). During anatexis, the Li
70 content of a melt is controlled both by the breakdown of these minerals, and by the partitioning
71 of Li between restitic minerals and melt as they re-equilibrate. We examined Li mineral–melt
72 partitioning during crustal anatexis via a batch melting geochemical model, which assumes that
73 generated melt remains in equilibrium with the source rock until extraction (Rosenberg and
74 Handy, 2005); an assumption validated in experimental studies (e.g., Acosta-Vigil et al., 2012).
75 The onset of melting, as well as the stability and thus presence of restitic minerals in equilibrium
76 with the melt, depends on the source composition and thermobarometric conditions of melting.
77 As such, we performed Gibbs free energy minimization calculations using the petrological
78 modeling program Theriak-Domino (De Capitani and Petrakakis, 2010) to determine the stable
79 mineral–silicate melt assemblages at different pressure (P , i.e. depth) and temperature (T)
80 conditions within the continental crust for two putative metasedimentary source rocks: the
81 average metapelite of Ague (1991) and a greywacke (Composition I of Pettijohn (1963)).
82 Although Li contents vary between metasedimentary rocks, for ease of comparison we assume
83 both compositions have a starting Li composition of 125.5 ppm, the average of 11,634
84 siliciclastic sedimentary rocks worldwide (see Supplementary Material).

85 We calculated P – T phase diagrams for both metasedimentary protoliths and examined the
86 crystallized products of extracted melts. Initial anatexis was examined along isobaric heating
87 paths at 3 kbar (~9 km depth, i.e., intrusion-related heating) and 8 kbar (~24 km, i.e., a standard
88 orogenic geotherm intersecting the solidus) under both dehydration melting (minimal saturation)
89 and flux melting scenarios to quantify how Li behaves during partial melting. Our approach
90 allowed the calculation of changes in melt Li content during crustal anatexis and then the

91 behavior of that melt fraction after extraction (set at 7 vol. % melt, the threshold at which melt
92 can escape its source, after Rosenberg and Handy, 2005).

93 Melt Li concentration was then modeled for two end-member scenarios: (1) the melt
94 extracted undergoes fractional crystallization in a closed system; and (2) the resulting extracted
95 melt crystallizes to form a granitic body which then undergoes a second (later) stage of anatexis.
96 Bulk Li partition coefficients for fractional crystallization were calculated using stable
97 assemblages present at the solidus and published mineral/melt partition coefficients. All models
98 were run through TDMelts (Koopmans et al., 2023) with the setup described in the
99 Supplementary Material.

100 During melting, both metasedimentary compositions (Figure 1a and Supplementary
101 Material) stabilize cordierite and biotite at low pressures, whereas muscovite and biotite are
102 stable at higher pressures. Figure 1 (b) shows the predicted partitioning of Li between
103 metasediment-derived melt and residuum for both starting compositions. At fluid-present
104 conditions, the solidus occurs between 660 and 690 °C and the release of Li into the melt is
105 largely controlled by the initial breakdown of muscovite and later breakdown of biotite.

106 Metapelites are typically enriched in Al compared to greywackes and stabilize higher
107 proportions of cordierite and mica at equivalent P - T conditions. At equivalent pressures,
108 greywacke-derived melts contain higher Li contents (by a factor of 1.3–2.1) than metapelite-
109 derived melts (Figure 1b); this difference is amplified at higher pressure due to the extended
110 stability of mica compared to cordierite.

111 Micas are the main hosts of Li in the subsolidus, and our models confirm that Li
112 enrichment during partial melting of metasedimentary rocks is primarily controlled by biotite and
113 muscovite stability, with cordierite having a minor influence, and feldspar playing an

114 insignificant role (Figure 1), agreeing with previous work (Kunz et al., 2022; Knoll et al., 2023).
115 Li is released into the melt upon mica breakdown, but importantly, the persistence of micas
116 during melting sequesters Li and serves to inhibit melt Li enrichment.

117 At a melt proportion of ~7 vol.%, we calculate maximum Li concentrations of 411 ppm
118 at 788 °C and 538 ppm at 785 °C for metapelites and metagreywackes, respectively. These
119 values represent a potential maximum Li enrichment factor of ~4.3 at extraction compared to the
120 source. Additionally, flux melting (i.e., ingress of external H₂O) also serves to depress melt Li
121 enrichment under all conditions, largely due to the higher proportion of micas present at melt
122 extraction conditions that have not broken down during melting reactions, although we note
123 melts are extractable at a significantly lower temperature (Figure 1b).

124 Fractional crystallization (our scenario 1) during cooling may further enrich the melt
125 phase in incompatible elements including Li. Modeled Rayleigh fractionation trends for melts
126 extracted at the 7 vol. % threshold are shown in Figure 2. In all cases, the concentration of Li
127 reaches 800–1800 ppm at 75% fractionation and 1500–3400 ppm at extreme fractionation
128 conditions (Zhao et al., 2022), still below the minimum saturation point for spodumene.
129 Spodumene saturation is only achieved at low pressure (3 kbar) during the final stages of
130 crystallization (Figure 2), when the melt fraction is reduced below 5 vol. %, a scenario which is
131 not physically extractable (Vigneresse et al., 1996).

132 Alternatively (scenario 2), the melt produced during anatexis of a metasedimentary
133 protolith may crystallize as a granitic body in the crust and experience a separate, later stage of
134 melting. We modeled the remelting of the granitic compositions produced through primary
135 anatexis (Figure 1c, d) to calculate potential second stage melt Li concentrations. In this
136 scenario, melt first appears between 640 °C and 675 °C, and coexists with a smaller proportion

137 of micas (<8 wt. %) relative to metasedimentary rocks, and no stable cordierite in any of the
138 modeled scenarios (Figure 1c). Accordingly, the secondary melting stage generates significantly
139 higher melt Li concentrations of 3590–7496 ppm at a 7 vol. % extraction point (Figure 1d), equal
140 to a potential Li enrichment factor of ~14.2 (Figures 1d, 3). These results importantly indicate
141 that a second stage of melting substantially enriches Li; in two stages driving Li concentration
142 from 125.5 to 7496 ppm, with the resultant secondary melts having economic potential without
143 invoking fractional crystallization.

144

145 **MULTI-STEP DISTILLATION MODEL FOR LI PEGMATITES**

146 Our results show that partial melting of typical metasedimentary sources followed by closed-
147 system fractional crystallization of those melt fractions cannot concentrate Li to the saturation
148 limit required (>5000 ppm) to generate a large zone of Li-aluminosilicates within a pegmatite.
149 Thus, production of a melt capable of saturating Li ore minerals in economic quantities within a
150 single stage melt scenario would require a rare, extremely enriched protolith (e.g., 1160 ppm in
151 the metasedimentary rock). While such concentrations have been documented in reworked Li-
152 rich volcanic sediments (e.g., Kadir et al., 2023), they are typically not documented near Li-rich
153 pegmatite provinces (e.g., Roda Robles et al., 1999) and therefore their role in Li pegmatite
154 formation is equivocal. By contrast, additional processing (i.e., re-melting) of a package of
155 continental crust can increase the Li concentration in a second-generation in order to allow
156 spodumene/petalite saturation very early in the fractionation history, obviating the need for
157 extensive fractional crystallization.

158 We therefore propose the following petrogenetic model for anatectic-origin Li pegmatites
159 with economic potential (Figure 4):

- 160 (1) Partial melting of a metasedimentary succession during prograde metamorphism,
161 which produces a granitic melt that is modestly enriched in Li;
162 (2) This melt crystallizes as a granitic intrusion structurally above the migmatite zone;
163 (3) A subsequent melting event, either an extension of the initial metamorphic event or
164 later during an unrelated orogenic cycle, reheats and remelts the granite forming a highly
165 enriched melt that ultimately crystallizes as a Li-rich pegmatite.

166 Our two-stage anatectic model indicates that the size of the pegmatite generated is approximately
167 200 times smaller than the metasedimentary protolith; for example, a deposit the size of Tanco
168 (0.021 km³, Stilling et al., 2006) likely formed from an initial metasedimentary package of c. 4.5
169 km³.

170 This mechanism also accounts for two particular features of pegmatites. Firstly,
171 pegmatites can be unzoned with economic minerals homogeneously distributed throughout,
172 requiring Li-bearing minerals to crystallize from the margin inwards (e.g., Kings Mt pegmatites;
173 Swanson, 2012); Mt Cattlin pegmatites, Sweetapple et al., 2019). This suggests the emplaced
174 melt has sufficiently high Li concentrations prior to crystallization.

175 Secondly, where pegmatite fields have a spatial relationship with granites, they are often
176 significantly younger (e.g., Stilling et al., 2006), which is at odds with arguments for the rapid
177 crystallization of pegmatites from the granitic melt when standard magmatic fractionation is
178 invoked (Simmons and Webber, 2008). Alternatively, many orogenic events are long-lived and
179 experience multiple cycles of melting (e.g., Mulcahy et al., 2014). Together, this suggests the
180 possibility of granites remelting as a mechanism for pegmatite genesis (e.g., Issia Zone, Brou et
181 al., 2022).

182 A multi-step anatectic model for the formation of Li pegmatites therefore satisfies these
183 geochemical and geochronological constraints, providing an efficient mechanism to elevate Li
184 concentrations and generate economic Li deposits.

185

186 **ACKNOWLEDGMENTS**

187 We thank delegates at the Maine Pegmatite Workshop, 2022, for fruitful discussions that
188 inspired this work. This work was funded by a National Environmental Research Council, UK
189 grant (no. NE/S007474/1) awarded to LK, a Natural Science and Engineering of Canada
190 Discovery Grant to RL, and a Mitacs Accelerate Award to LG and RL for intern CB. We thank
191 Kathryn Goodenough and two anonymous reviewers for their insightful comments, and Andrew
192 Barth for editorial handling of the manuscript.

193

194 **REFERENCES CITED**

- 195 Acosta-Vigil, A., Buick, I., Cesare, B., London, D., and Morgan, G.B., 2012, The Extent of
196 Equilibration between Melt and Residuum during Regional Anatexis and its Implications
197 for Differentiation of the Continental Crust: a Study of Partially Melted Metapelitic
198 Enclaves: *Journal of Petrology*, v. 53, p. 1319–1356.
- 199 Ague, J.J., 1991, Evidence for major mass transfer and volume strain during regional
200 metamorphism of pelites: *Geology*, v. 19, p. 855–858.
- 201 Bradley, D., and Mccauley, A., 2017, A Preliminary Deposit Model for Lithium-Cesium-
202 Tantalum (LCT) Pegmatites: US Geological Survey, doi:10.3133/ofr20131008.
- 203 Brou, J.K., Van Lichtervelde, M., Kouamelan, N.A., Baratoux, D., and Thébaud, N., 2022,
204 Petrogenetic relationships between peraluminous granites and Li- Cs-Ta rich pegmatites
205 in south Issia zone (Central-West of Côte d'Ivoire): *Petrography, Mineralogy,*
206 *Geochemistry and zircon U–Pb Geochronology: Mineralogy and Petrology*, v. 116, p.
207 443–471.
- 208 Cameron, E.N., Jahns, R.H., McNair, A.H., and Page, L.R., 1949, Internal Structure of Granitic
209 Pegmatites: Society of Economic Geologists.

- 210 Černý, P., 1991, Rare-element Granitic Pegmatites. Part II: Regional to Global Environments
211 and Petrogenesis: GSA today: a publication of the Geological Society of America,
212 <https://journals.lib.unb.ca/index.php/GC/article/view/3723> (accessed March 2023).
- 213 Černý, P., Blevin, P.L., Cuney, M., and London, D., 2005, Granite-Related Ore Deposits:
214 Economic Geology, p. 337–370.
- 215 De Capitani, C., and Petrakakis, K., 2010, The computation of equilibrium assemblage diagrams
216 with Theriak/Domino software: The American mineralogist, v. 95, p. 1006–1016.
- 217 Dittrich, T., Seifert, T., Schulz, B., Hagemann, S., Gerdes, A., and Pfänder, J., 2019, Introduction
218 to Archean Rare-Metal Pegmatites: , p. 1–21.
- 219 Jahns, R.H., 1953, The genesis of pegmatites: I. Occurrence and origin of giant crystals: The
220 American mineralogist, v. 38, p. 563–598.
- 221 Kadir, S., Kūlah, T., Erkoyun, H., Helvacı, C., Eren, M., and Demiral, B., 2023, Mineralogy,
222 geochemistry, and genesis of lithium-bearing argillaceous sediments associated with the
223 Neogene Bigadiç borate deposits, Balıkesir, western Anatolia, Türkiye: Applied clay
224 science, v. 242, p. 107015.
- 225 Knoll, T., Huet, B., Schuster, R., Mali, H., Ntaflos, T., and Hauzenberger, C., 2023, Lithium
226 pegmatite of anatectic origin - A case study from the Austroalpine Unit Pegmatite
227 Province (Eastern European Alps): geological data and geochemical model: Ore Geology
228 Reviews, p. 105298.
- 229 Koopmans, L., Palin, R.M., and Gardiner, N.J., 2023, TDMelts: A Theriak-Domino Wrapper for
230 2-dimensional batch melting models, *in* Goldschmidt 2023 Conference,
231 GOLDSCHMIDT,
232 <https://conf.goldschmidt.info/goldschmidt/2023/meetingapp.cgi/Paper/20404> (accessed
233 August 2023).
- 234 Kunz, B.E., Warren, C.J., Jenner, F.E., Harris, N.B.W., and Argles, T.W., 2022, Critical metal
235 enrichment in crustal melts: The role of metamorphic mica: Geology, v. 50, p. 1219–
236 1223.
- 237 London, D., 2014, A petrologic assessment of internal zonation in granitic pegmatites: Lithos, v.
238 184–187, p. 74–104.
- 239 London, D., 1984, Experimental phase equilibria in the system LiAlSiO₄–SiO₂–H₂O: a
240 petrogenetic grid for lithium-rich pegmatites: The American mineralogist, v. 69, p. 995–
241 1004.
- 242 Maneta, V., Baker, D.R., and Minarik, W., 2015, Evidence for lithium-aluminosilicate
243 supersaturation of pegmatite-forming melts: Contributions to mineralogy and petrology.
244 Beitrage zur Mineralogie und Petrologie, v. 170, p. 4.

- 245 Mulcahy, S.R. et al., 2014, Multiple migmatite events and cooling from granulite facies
246 metamorphism within the Famatina arc margin of northwest Argentina: *Tectonics*, v. 33,
247 p. 1–25.
- 248 Müller, A., Romer, R.L., and Pedersen, R.B., 2017, The sveconorwegian pegmatite province -
249 thousands of pegmatites without parental granites: *Canadian mineralogist*, v. 55, p. 283–
250 315.
- 251 Pettijohn, F.J., 1963, Chemical composition of sandstones, excluding carbonate and volcanic
252 sands: USGS, 1–21 p.
- 253 Roda Robles, E., Pesquera Perez, A., Velasco Roldan, F., and Fontan, F., 1999, The granitic
254 pegmatites of the Fregeneda area (Salamanca, Spain): characteristics and petrogenesis:
255 *Mineralogical magazine*, v. 63, p. 535–558.
- 256 Rosenberg, C.L., and Handy, M.R., 2005, Experimental deformation of partially melted granite
257 revisited: implications for the continental crust: *Journal of Metamorphic Geology*, v. 23,
258 p. 19–28.
- 259 Shaw, R.A., Goodenough, K.M., Roberts, N.M.W., Horstwood, M.S.A., Chenery, S.R., and
260 Gunn, A.G., 2016, Petrogenesis of rare-metal pegmatites in high-grade metamorphic
261 terranes: A case study from the Lewisian Gneiss Complex of north-west Scotland:
262 *Precambrian research*, v. 281, p. 338–362.
- 263 Simmons, W.B., Foord, E.E., Falster, A.U., and King, V.T., 1995, Evidence for an anatectic
264 origin of granitic pegmatites, western Maine, USA, *in* Geological Society of America
265 Annual Meeting, New Orleans Abstracts, A411, p. 27.
- 266 Simmons, W.B. “skip,” and Webber, K.L., 2008, Pegmatite genesis: state of the art: *European*
267 *Journal of Mineralogy*, v. 20, p. 421–438.
- 268 Simons, B., Andersen, J.C.Ø., Shail, R.K., and Jenner, F.E., 2017, Fractionation of Li, Be, Ga,
269 Nb, Ta, In, Sn, Sb, W and Bi in the peraluminous Early Permian Variscan granites of the
270 Cornubian Batholith: Precursor processes to magmatic-hydrothermal mineralisation:
271 *Lithos*, v. 278–281, p. 491–512.
- 272 Stewart, D.B., 1978, Petrogenesis of lithium-rich pegmatites: *The American mineralogist*, v. 63,
273 p. 970–980.
- 274 Stilling, A., Cerny, P., and Vanstone, P.J., 2006, THE TANCO PEGMATITE AT BERNIC
275 LAKE, MANITOBA. XVI. ZONAL AND BULK COMPOSITIONS AND THEIR
276 PETROGENETIC SIGNIFICANCE: *Canadian mineralogist*, v. 44, p. 599–623.
- 277 Swanson, S.E., 2012, MINERALOGY OF SPODUMENE PEGMATITES AND RELATED
278 ROCKS IN THE TIN–SPODUMENE BELT OF NORTH CAROLINA AND SOUTH
279 CAROLINA, USA: *Canadian mineralogist*, v. 50, p. 1589–1608.

- 280 Sweetapple, M.T., Grigson, M.W., Tornatora, P., and Urgine, S., 2019, The Archean Mt. Cattlin
281 spodumene pegmatite group and 3D geochemical mapping of large “unzoned” pegmatites
282 of economic significance: *Canadian mineralogist*, v. 57, p. 803–805.
- 283 Taylor, S.R., and McLennan, S.M., 2003, Chemical Composition and Element Distribution in the
284 Earth’s Crust, *in* Meyers, R.A. ed., *Encyclopedia of Physical Science and Technology*
285 (Third Edition), New York, Academic Press, p. 697–719.
- 286 U.S. Geological Survey, 2023, Mineral commodity summaries 2023: US Geological Survey,
287 doi:10.3133/mcs2023.
- 288 Vigneresse, J.L., Barbey, P., and Cuney, M., 1996, Rheological transitions during partial melting
289 and crystallization with application to felsic magma segregation and transfer: *Journal of*
290 *Petrology*, v. 37, p. 1579–1600.
- 291 Zhao, P., Chu, X., Williams-Jones, A.E., Mao, J., and Yuan, S., 2022, The role of phyllosilicate
292 partial melting in segregating tungsten and tin deposits in W-Sn metallogenic provinces:
293 *Geology*, v. 50, p. 121–125.
- 294
- 295

296 Figure 1. Representative results of petrologic modeling of a metasedimentary rock (a, b, here the
297 greywacke at 8 kbar) and granite (c, d, sourced from greywacke at 8 kbar) composition
298 undergoing isobaric heating. Modebox diagrams (a, c) show the equilibrium assemblages across
299 the modelled temperature range. The dashed lines highlight the stable assemblage under flux
300 melting conditions. The graph in (b) traces the concentration of lithium in the melt component of
301 the modelled metasedimentary scenarios. (d) as (b), though of the melt components of the
302 corresponding metasedimentary rocks of (b). Stars denote melt extraction points for each
303 condition, where Flux corresponds to flux melting and Sat. corresponds to dehydration melting.
304 Details of the modelling method are provided in the Supplementary Material. Mineral
305 abbreviations: Amph: amphibole; Bt: biotite; Cd: cordierite; Fsp: feldspar; Gt: garnet; Kfs:
306 Alkali feldspar; Mu: muscovite; Pl: plagioclase; Opx: orthopyroxene; Q: quartz.

307 Figure 2. The behavior of lithium (Li) in the extracted melt during Rayleigh fractionation. The
308 initial Li content of each melt corresponds to the concentration of Li at extraction in each of the
309 modelled scenarios. The partition coefficients are taken from the model near the solidus of each
310 individual melt. The particle-locking threshold (PLT) of Vigneresse et al. (1996) and the extreme
311 fractionation boundary of Zhao et al. (2022) are highlighted, as well as the minimum threshold
312 for spodumene saturation (Maneta et al., 2015).

313 Figure 3. Evolution of Li concentrations during melting and fractionation of melt components
314 generated during crustal anatexis – with the spodumene saturation boundary highlighted (Maneta
315 et al., 2015). After initial melt extraction, the granite either: 1) undergoes fractional
316 crystallization (hollow symbols, the compositions of fractional crystallization was taken as the
317 composition at 90% crystallization); or (2) is assumed to crystallize and then remelted and
318 extracted at the 7% melt (filled shapes).
319

320 Figure 4. Schematic petrogenetic model for generating lithium (Li)-rich pegmatites in the via
321 crustal anatexis. (A) Partial melting of a metasedimentary rock generates melt lenses, which
322 periodically lose melt. (B) grain-scale diagram visualizing melt films connecting and driving
323 melt out of the system in (A). The breakdown of hydrous phases and mineral-melt diffusion
324 controls the Li budget of the resultant melt. (C) The melt accumulates and crystallizes as a
325 granite structurally above the anatectic zone. (D) A subsequent melting event, either associated
326 with the primary metamorphic event, or during a later orogenic cycle melts the granite,
327 generating Li-rich pegmatites in their vicinity.

328 ¹Supplemental Material. *Description of model setup and geochemical database used*. Please visit
329 <https://doi.org/10.1130/XXXX> to access the supplemental material, and contact
330 editing@geosociety.org with any questions.

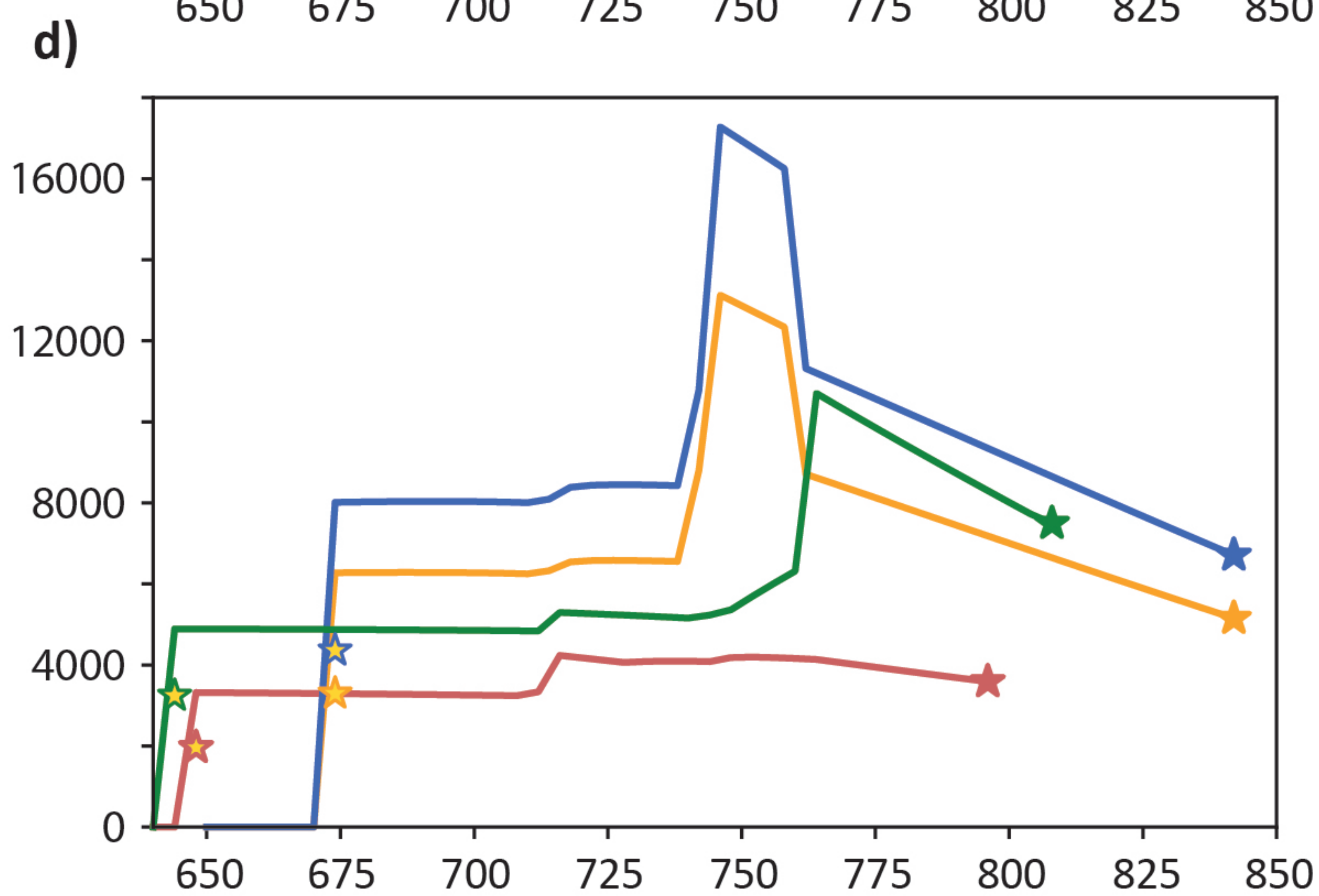
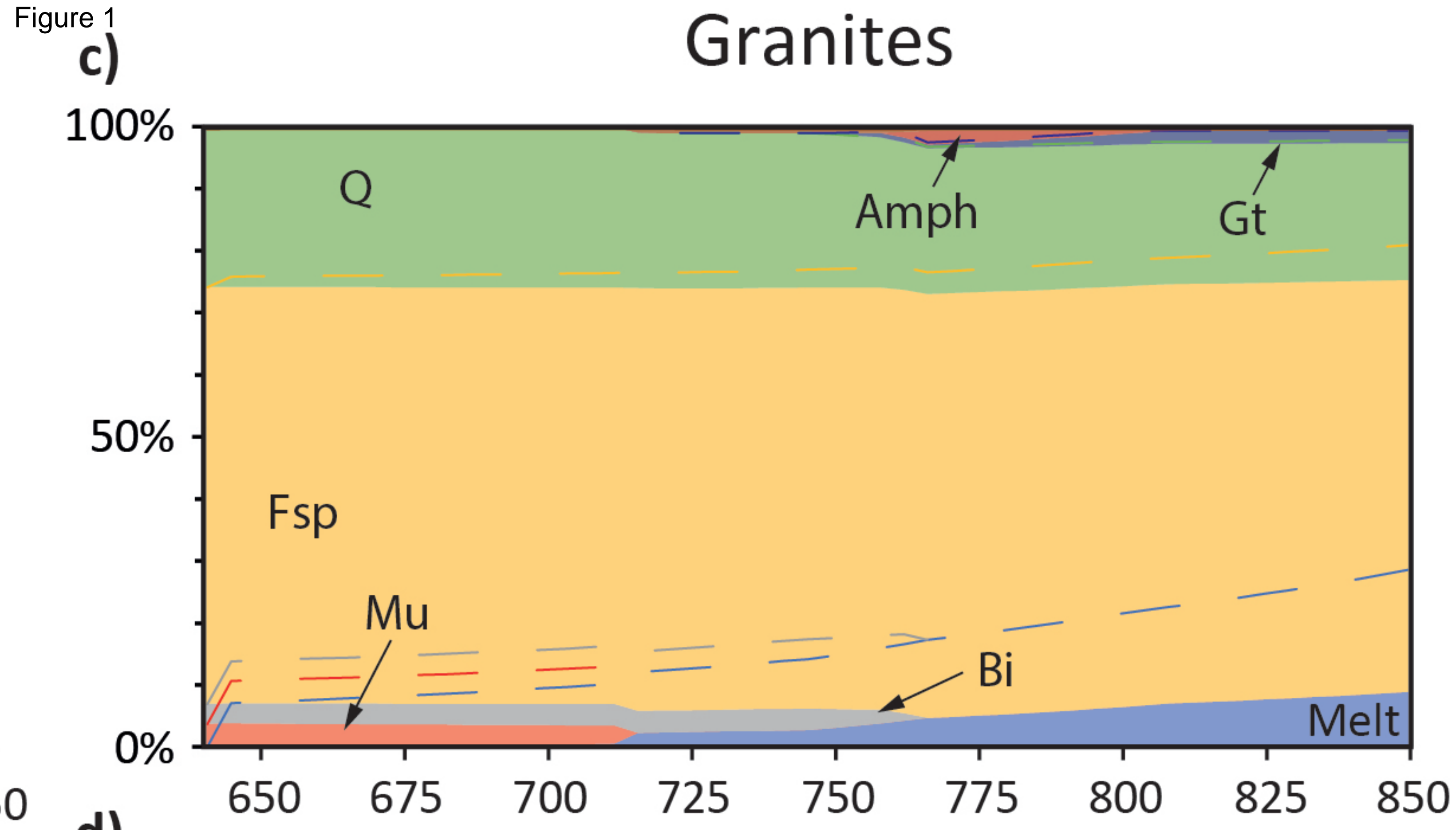
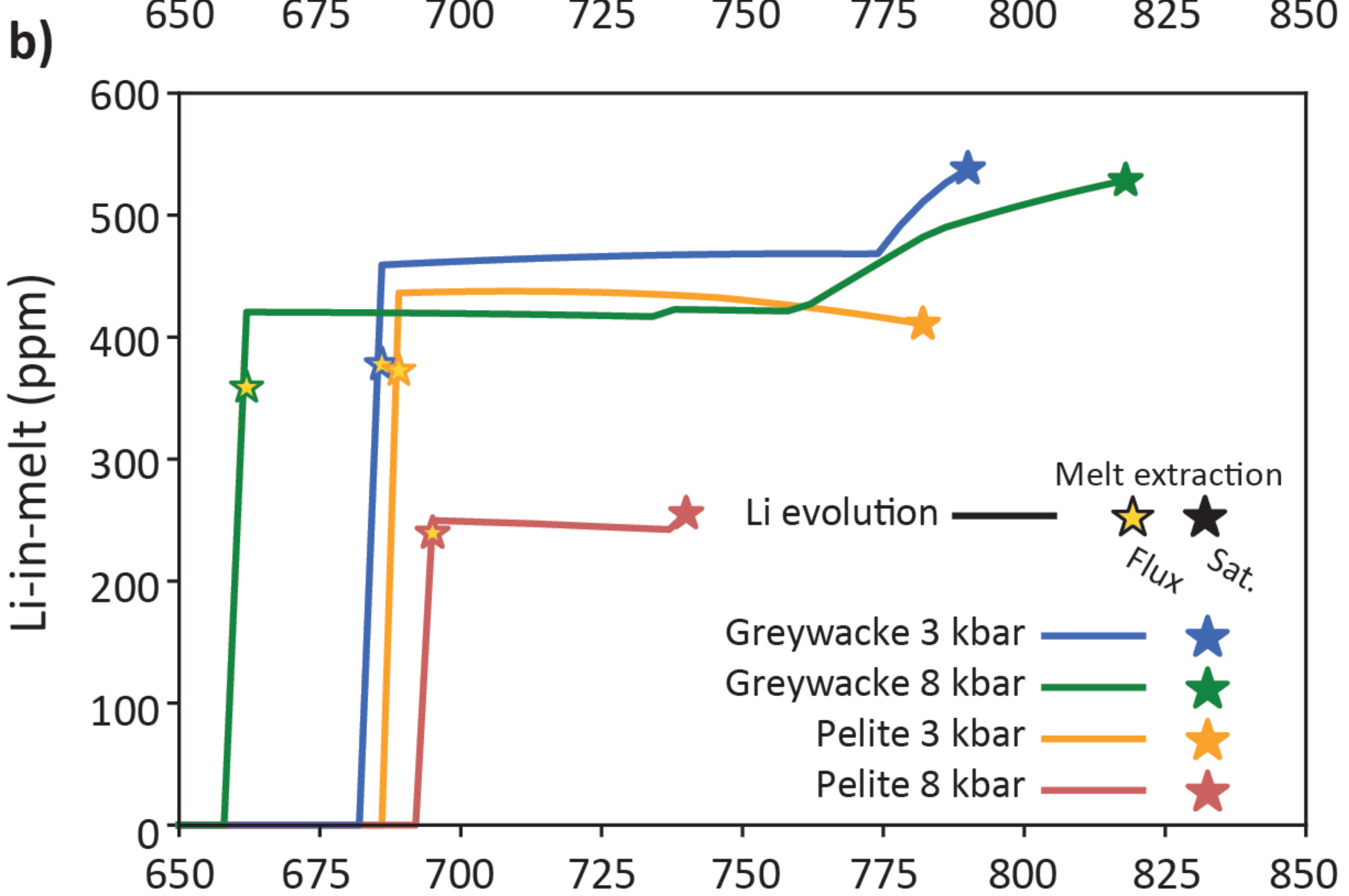
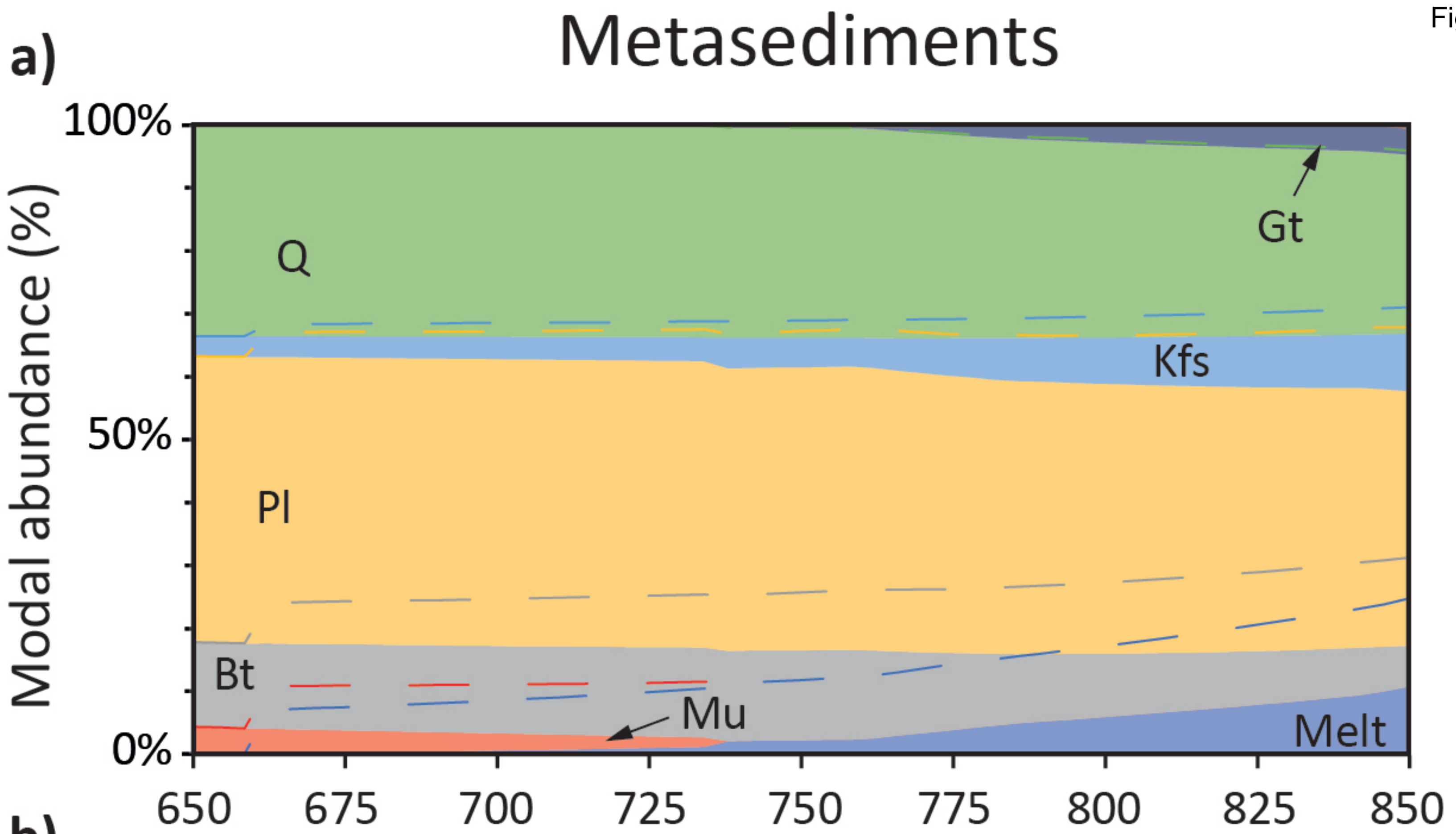


Figure 2

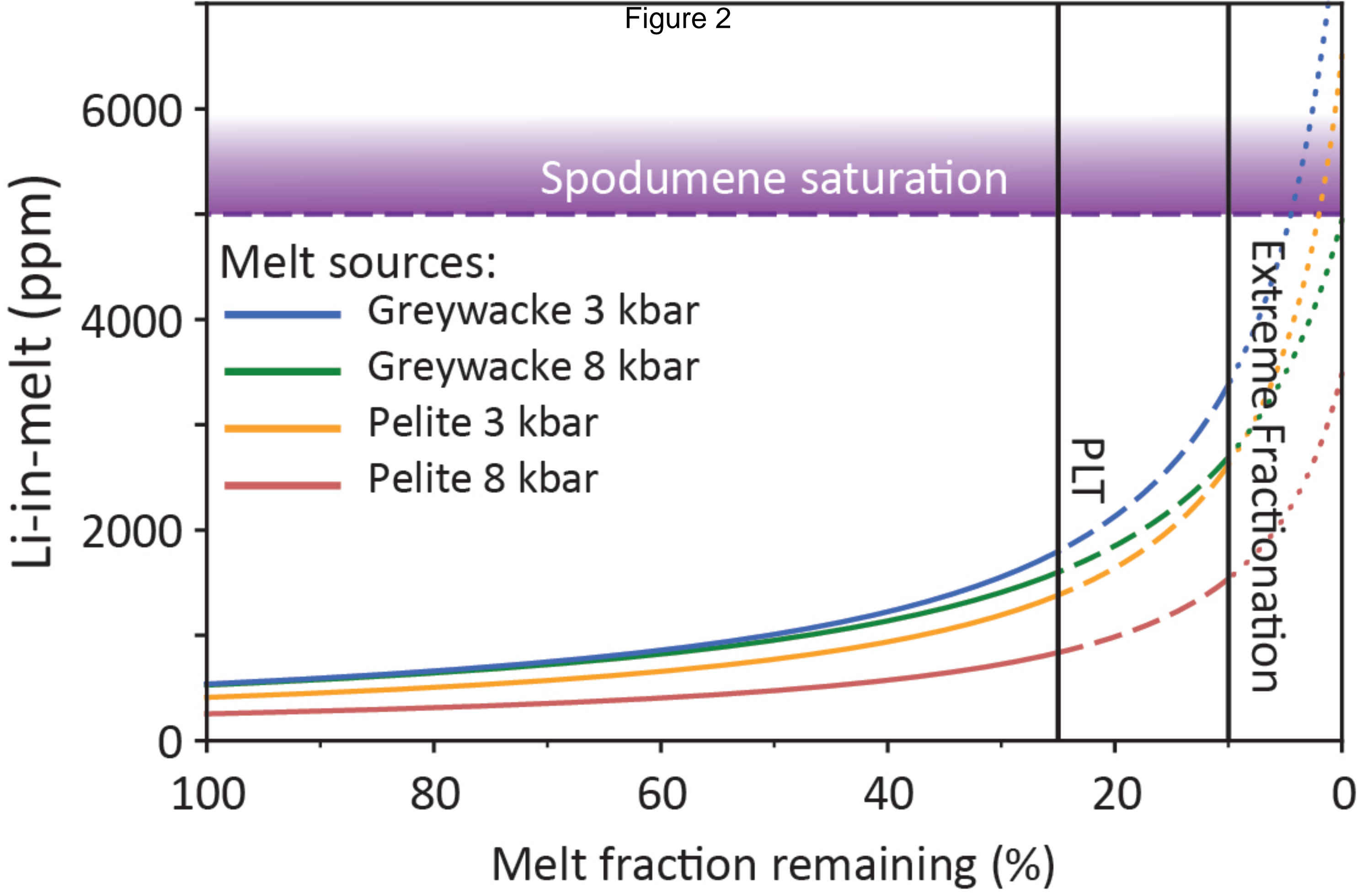
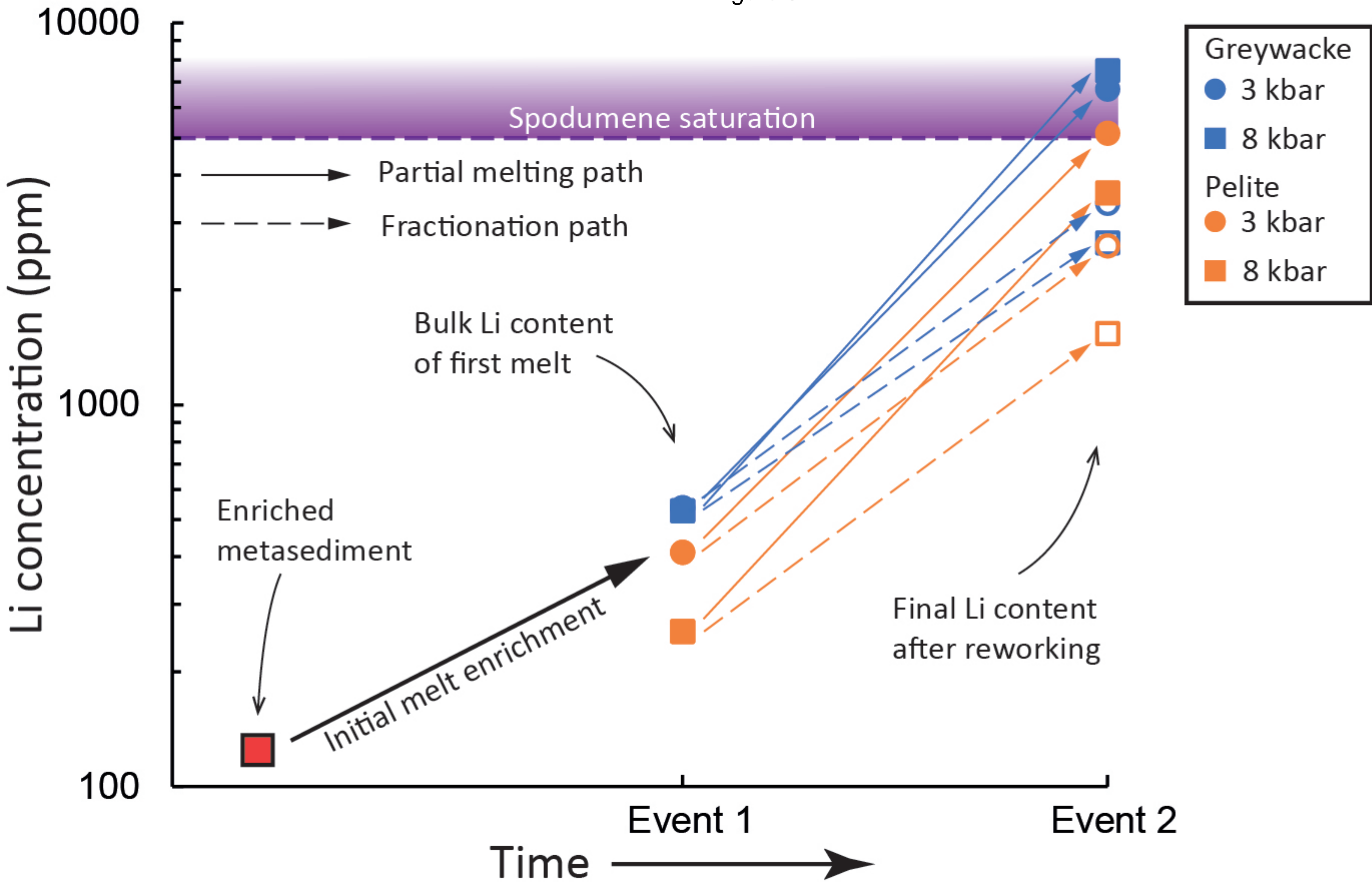
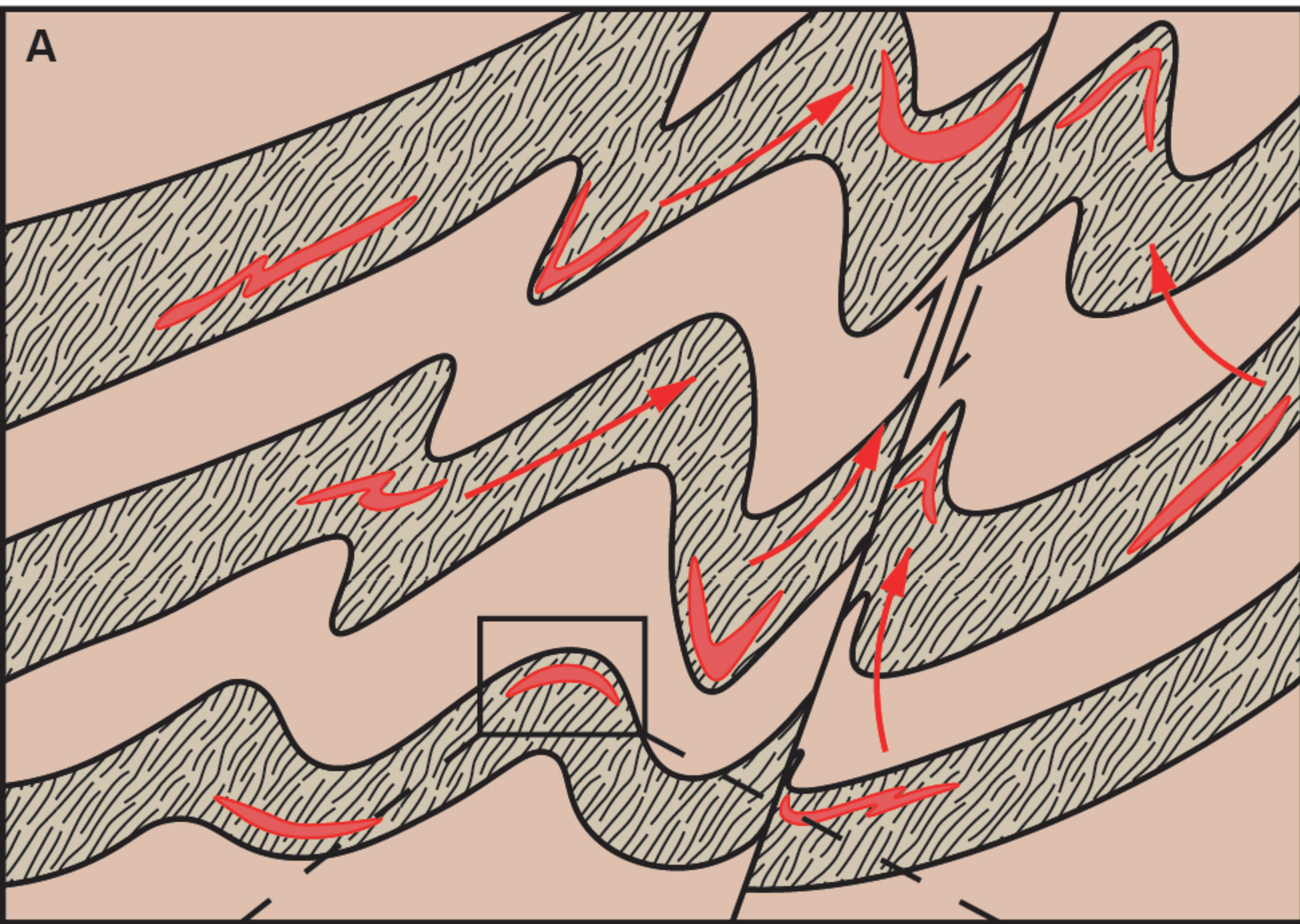


Figure 3

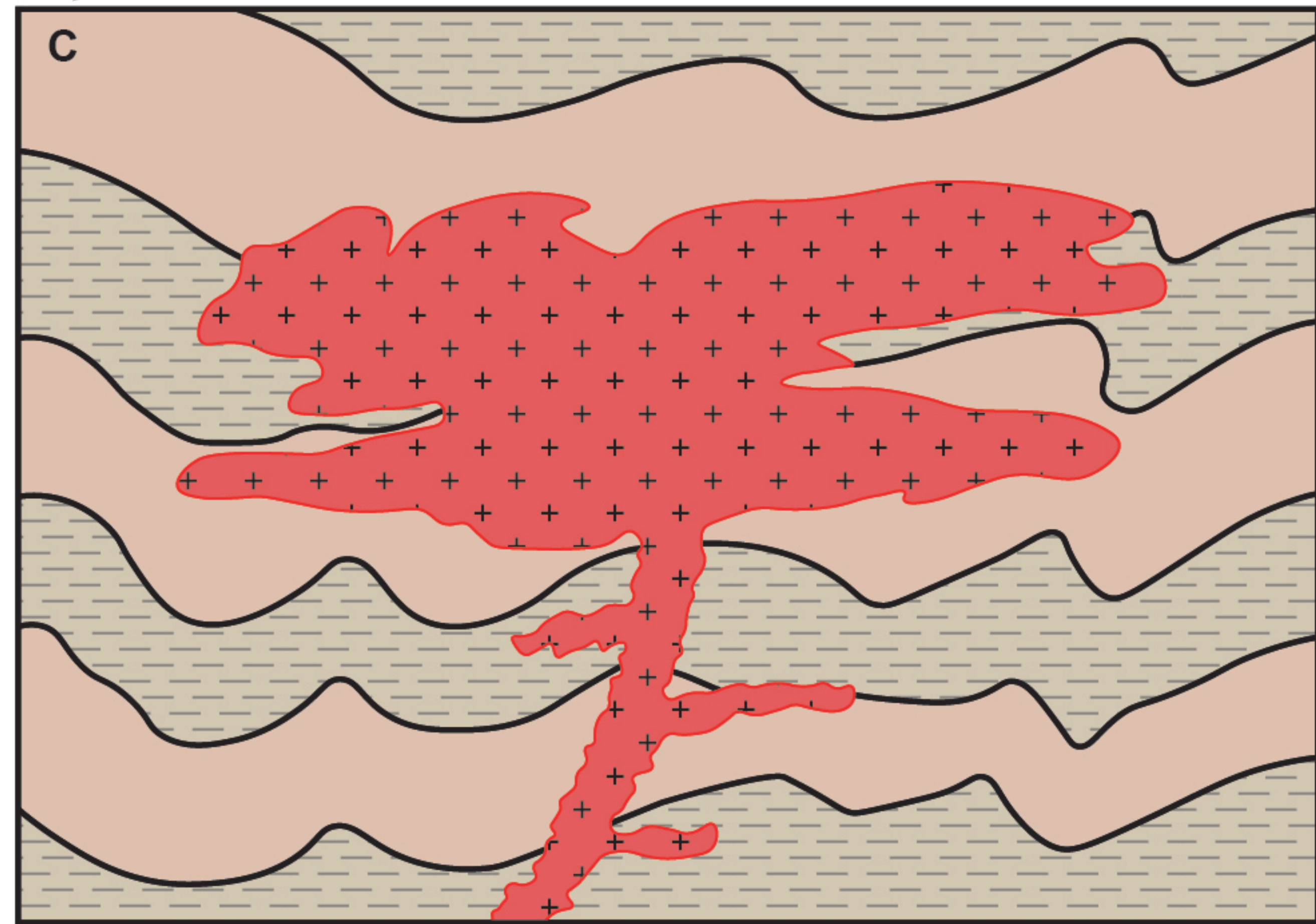


Step 1 - Anatexis of metasedimentary rocks

Li in metasedimentary rocks = 125 ppm



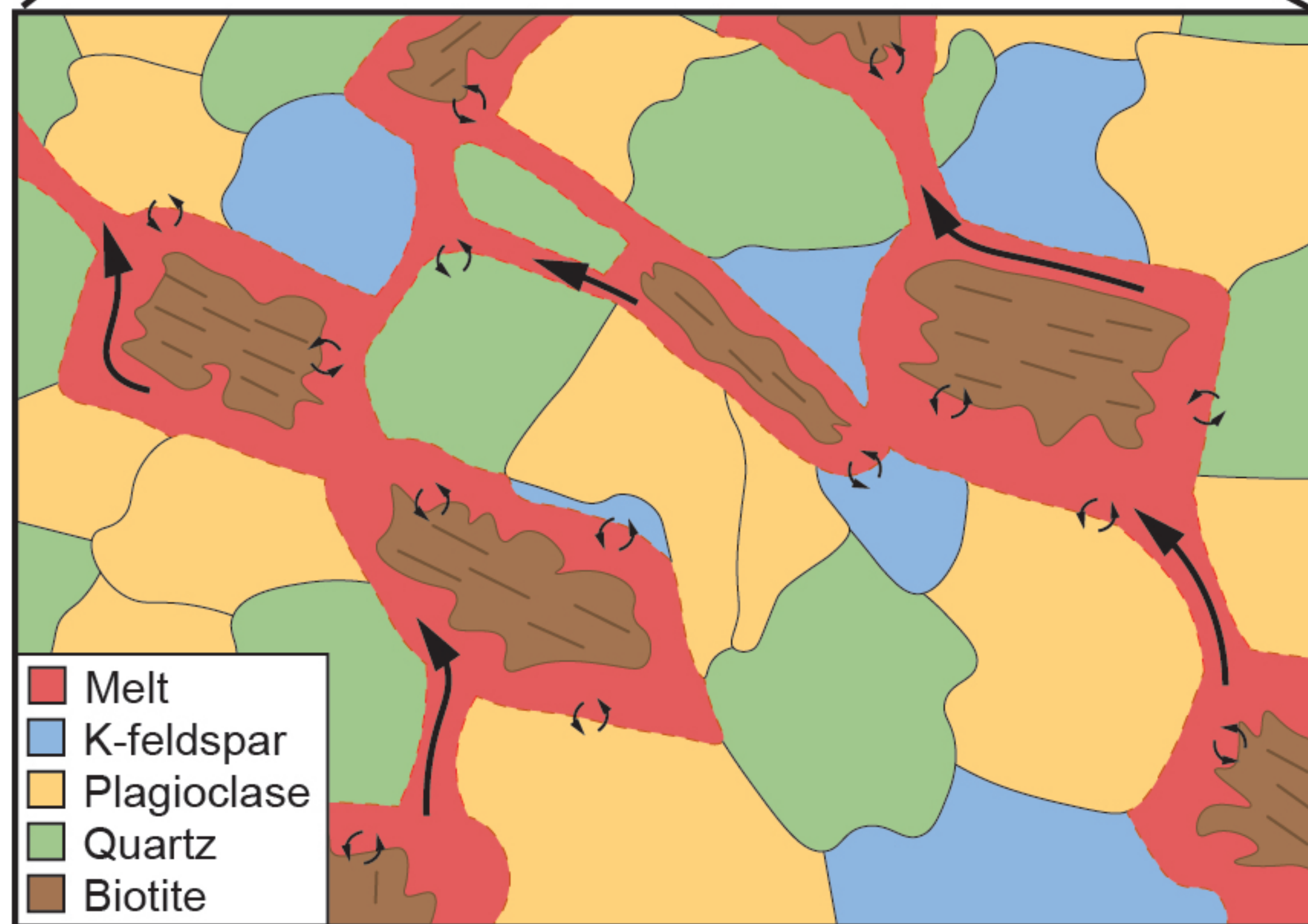
Li in melt = 255-538 ppm



Step 2 - Anatexis of granites



B



Li in pegmatites = 3590-7496 ppm

